

Nanometer Spatial Resolution Achieved in Hard X-ray Imaging and Laue Diffraction Experiments

Donald H. Bilderback,* Stephen A. Hoffman, Daniel J. Thiel

Tapered glass capillaries have successfully condensed hard x-ray beams to ultrasmall dimensions providing unprecedented spatial resolution for the characterization of materials. A spatial resolution of 50 nanometers was obtained while imaging a lithographically prepared gold pattern with x-rays in the energy range of 5 to 8 kiloelectron volts. This is the highest resolution scanning x-ray image made to date with hard x-rays. With a beam 360 nanometers in diameter, Laue diffraction was observed from the smallest sample volume ever probed by x-ray diffraction, 5×10^{-3} cubic micrometers.

X-ray techniques such as diffraction, spectroscopy, small-angle x-ray scattering, fluorescence, and others have yielded important structural information about the nature of crystals, fibers, powders, and composite materials. For instance, the molecular structure of biological assemblies such as the human cold virus (1) and the enzyme HIV-1 reverse transcriptase (2) have been determined from x-ray diffraction patterns. Also, x-ray spectroscopy has been used to probe electronic structure within a variety of materials, such as high-temperature superconductors (3). A major limitation to most x-ray studies, however, is that they typically require relatively large samples (0.1 to 10 mm) containing many atoms, molecules, or virus assemblies.

There is considerable interest in probing the structure of samples significantly less than 0.1 mm across. For instance, x-ray microbeam techniques may yield information about the ordering of atoms in the immediate vicinity of a grain boundary in an alloy or may help to determine the difference in structure between surface and interior regions of a polymer fiber that is only a few micrometers in diameter. It is difficult to obtain spatially resolved information of this type from crystallographic or spectroscopic measurements by conventional techniques because specimens having millimeter dimension must ordinarily be completely illuminated by the x-rays to detect a measurable signal. Thus, microbeam experiments require both a very small beam size and a very high x-ray intensity.

Microfocusing techniques are very well developed in the case of soft x-rays (energies < 4 keV). For example, Anderson and Kern (4) demonstrated 30-nm spatial resolution using zone plates with 30 Å wavelength (400-eV) x-rays. However, low-energy x-ray beams cannot access the distinct inner-shell absorption edges of most ele-

ments of the periodic chart and cannot yield sufficient diffraction information for quantitative structural determination. Also, low-energy x-rays do not penetrate as far into thicker or more dense specimens as do high-energy x-rays. It is advantageous, therefore, to obtain sample characterization information with hard x-ray microbeams.

Some examples can be given to show the breadth of recent x-ray microbeam developments. Using a thin, hollow microchannel plate as a grazing incidence x-ray reflector, Chapman *et al.* (5) made a 150- μm -diameter beam at 8 keV. In a different approach, Kumakhov and Komarov (6) achieved beam sizes of 1 mm with a bundle of many curved polycapillary tubes that guided the x-rays to a focal spot. Carpenter *et al.* (7) have made a 10- μm -diameter x-ray beam using a single untapered glass capillary. Curved multilayer mirrors in the Kirkpatrick-Baez (KB) configuration (8) have produced a beam with a 2 μm by 2 μm cross section at 8.6 keV. Phase zone plates (9) have yielded a spot size of 0.65 μm by 0.65 μm cross section at 8 keV. Finally, Bragg-Fresnel lenses (10) have recently generated a 0.8- μm -diameter beam.

Another very successful approach to the creation of submicrometer beams has been to make x-ray concentrators based on the total external reflection of x-rays from the inside wall of tapered glass tubing. Although many experiments have been conducted in which x-rays have been successfully reflected down untapered hollow glass tubes, it was the work of Stern *et al.* (11) that first showed in a detailed manner the intensity gains possible by the tapering of the capillaries to compress the diameter of the x-ray beam. Subsequently, Engström *et al.* (12) and ourselves have made tapered x-ray capillaries with submicrometer exit openings. We have experimentally demonstrated that beams 0.1 μm in diameter can be obtained (13, 14) with intensity (x-rays per second per square micrometer) gains of up to 960 at 6 keV.

We made our tapered capillaries (Fig. 1) by heating a piece of leaded glass tubing

(density $\rho = 5.2$ g/cm³) in a vertical tube furnace to near the melting temperature and slowly drawing it to a needle-like point with a weight attached to the lower end. All rays pass through efficiently provided that the incidence angle of each x-ray does not exceed the critical angle of total reflection, θ_c [for materials with low atomic weights, $\theta_c = 1.64 \times 10^{-3} \lambda \sqrt{\rho}$, where θ_c is in radians, λ is the wavelength of the radiation in angstroms, and ρ is in grams per cubic centimeter (15); for leaded glass and 1 Å radiation, $\theta_c = 3.8$ mrad or 0.2 degrees].

One advantage of tapered glass capillaries over x-ray optics based on diffraction is their ability to concentrate wide-band polychromatic as well as monochromatic x-rays. Another advantage is that the size of the concentrated beam does not depend on the coherence of the x-rays as it does in the case of zone plates. Glass capillaries are actually nonimaging devices that have properties similar to those of the solar condensers described by Cooke *et al.* (16). Just as in the visible-light case where the lack of any imaging requirement allows concentrators to produce the highest intensity spots of solar light, we believe that the nonimaging capillary concentrators can yield the highest intensity spots of x-rays with low divergence beams from synchrotron radiation sources.

Experiments with tapered capillaries of various dimensions were conducted on the Cornell High-Energy Synchrotron Source (CHESS) bending magnet station B2 (critical energy $E_{\text{crit}} = 10$ keV, machine energy $E = 5.3$ GeV, current $I = 80$ mA) to demonstrate imaging and diffraction applications. In the imaging experiment, a lithographically deposited gold pattern with 300-nm-wide features was scanned in two dimensions through the concentrated x-ray beam while the transmission of x-rays

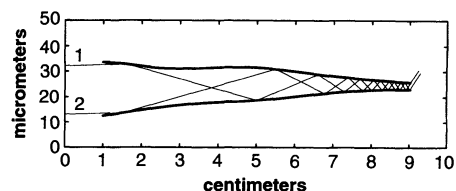


Fig. 1. Profile of the inner diameter (ID) of a capillary measured with an optical microscope. The entering ID is 22 μm and the exit ID is 3 μm . The calculated trajectories of two rays from a parallel x-ray beam are shown. Ray 1 undergoes 12 successive bounces with a net throughput of 57%, as calculated by a two-dimensional ray-tracing program that includes the x-ray reflectance for each bounce. Ray 2 undergoes 11 reflections with a net throughput of 61%. The average reflectivity per bounce exceeds 95%, and the total deflection angles are 2.3 and 2.2 mrad, respectively.

Cornell High Energy Synchrotron Source and the School of Applied and Engineering Physics, Cornell University, Ithaca, NY 14853.

*To whom all correspondence should be addressed.

through the sample was monitored (Fig. 2). The 300-nm separation of the features was easily resolved. Because the concentrated beam was considerably smaller than this separation, further investigation was made to reveal the actual beam size.

The diameter of the x-ray beam was less than two scan steps, or 100 nm, as determined from one-dimensional scans across the sharp edge of a gold line. Also, we observed that in a 50-nm distance, the scanning edge reduced the transmitted flux through the gold layer from 80% to 20%, a criterion commonly used to define the spatial resolution. These scanning measurements of beam size agree well with a separate optical determination of a 90-nm beam diameter, which we inferred by measuring the size of the outside diameter of the tip with an optical microscope and scaling by the wall thickness accordingly (17).

In summary, the beam diameter was

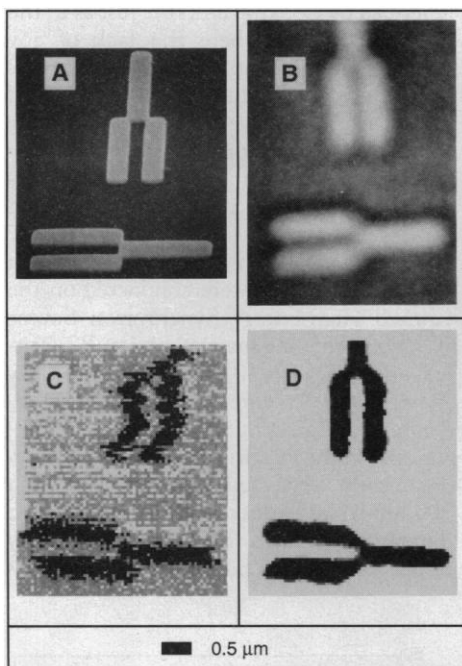


Fig. 2. Various images of a lithographically prepared test sample consisting of a 100-nm-thick gold pattern deposited on a 200-nm-thick Si_3N_4 substrate. The line widths of the features are 300 nm. (A) Scanning electron micrograph. (B) Optical image obtained with a visible-light microscope with a numerical aperture of 0.9. The image is blurred because the structure has features below the resolving power of the microscope. (C) Unprocessed x-ray absorption image. The image was formed from a two-dimensional scan consisting of 50 nm by 50 nm pixels. (D) X-ray image after processing. The data in each row were horizontally shifted to compensate for the effects of spatial drift (thermal, air currents, electronic, and so on). A median processor was then applied, which averages all pixel intensities located in a circle of radius 2 pixels.

determined to be 95 ± 5 nm. The error is based on the upper limit of 100 nm, given by two pixel steps in the image, and the lower limit of 90 nm, from the independent optical measurement. The spatial resolution was 50 nm, which is the highest resolution observed with hard x-rays.

Because this tapered capillary had an entrance inner diameter of 45 μm , the measured x-ray flux transmission and the exiting beam size determined above gave an intensity gain of 50. A more perfectly drawn capillary could have probably yielded 20 times more gain on a bending magnet source at CHESS and perhaps as much as 100 to 1000 times more gain on undulator-type synchrotron sources.

The x-ray beam leaving the capillary has a divergence of only a few milliradians and has the smallest diameter directly at the tip. The "depth of focus" for this optic is typically 20 to 100 times the tip diameter or 2 to 10 μm for the 100-nm beam diameter in this example.

Three transmission Laue patterns were

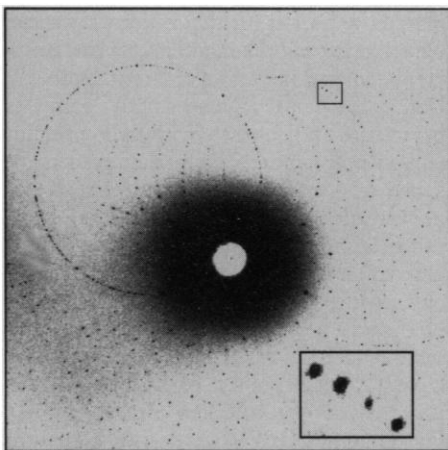
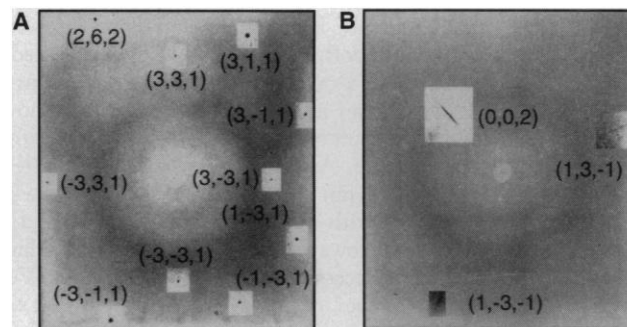


Fig. 3. Laue diffraction from a lysozyme crystal taken with a 5.6- μm -diameter x-ray beam. The divergence of the microbeam was 2.6 mrad as determined from the measured size of the diffraction spots on the film.

Fig. 4. Transmission Laue diffraction patterns taken with a 360-nm-diameter x-ray beam. The local areas around the spots have been individually enhanced to make them more visible and are labeled with Miller indices. (A) Laue pattern from a 4- μm -thick perfect crystal silicon wafer taken in a 10-s exposure. The round spot size is consistent with a microbeam divergence of 8 mrad. (B) Laue pattern from a 50-nm-thick single crystal gold foil.



taken to demonstrate the possibilities of obtaining diffraction information from tiny crystal volumes. In the first Laue experiment, a 150- μm -thick single crystal of lysozyme was placed a few micrometers away from a tapered capillary that created a 5.6- μm -diameter x-ray beam (5 to 25 keV). This is the smallest diameter x-ray beam yet used in protein crystallography experiments. We translated the sample 3 μm every 24 s during the 300-s exposure to minimize the radiation damage (in the future, a cryogenic cooling apparatus may alleviate this translation requirement). The diffraction pattern (Fig. 3) was recorded on Kodak DEF wet film located 11.5 cm away from the sample and showed structural resolution extending to 2.2 \AA . This experiment shows the promise of tapered capillaries in the study of biological materials that do not form the large crystals (100 μm or larger) needed for conventional x-ray crystallography.

In the second Laue experiment, another capillary that produced a 360-nm-diameter x-ray beam with an intensity gain of 31 was used. Ideal, round diffraction spots were recorded on Polaroid film (Fig. 4A) located 6 cm from a 4- μm -thick perfect crystal silicon wafer that was placed near the tip of the capillary.

In the third Laue experiment, the silicon wafer was replaced by a 50-nm-thick single crystal gold foil. Several diffraction streaks, instead of spots, were observed in a 10-min exposure (Fig. 4B). In the transmission Laue geometry, the diffraction spots from a perfect crystal map into streaks if the crystal is made up of many slightly misoriented diffracting domains (18). The streaks are consistent with a mosaic spread of several degrees and were observed with beam sizes ranging from 45 μm down to 360 nm. Because round diffraction spots were never observed, we conclude that the size of the mosaic diffracting domains is less than the beam size of 360 nm.

The illuminated volume from the gold

foil sample is $5 \times 10^{-3} \mu\text{m}^3$, the smallest single crystal volume studied by x-ray diffraction methods. This volume is a factor of 6 smaller than that investigated by Skelton *et al.* (19) ($3 \times 10^{-2} \mu\text{m}^3$) and one-fourth that studied by Ohsumi *et al.* (20) ($2 \times 10^{-2} \mu\text{m}^3$). In the latter two cases, the diffracting volume was determined by the volume of a tiny sample completely bathed by a much larger beam. However, for the study of small crystal volumes, our micro-beam technique improves the signal-to-background ratio, allowing the study of even smaller crystal volumes in the future.

At the present time, tapered capillaries are the only x-ray optical component producing nanometer spatial resolution with high-energy x-rays. We anticipate that many new experiments will be possible with these ultrasmall diameter x-ray beams.

REFERENCES AND NOTES

- M. G. Rossmann *et al.*, *Nature* **317**, 145 (1985).
- E. Arnold *et al.*, *ibid.* **357**, 85 (1992).
- J. M. Tranquada *et al.*, *ibid.* **337**, 720 (1989).
- E. H. Anderson and D. Kern, in *X-ray Microscopy III*, A. G. Michette, G. R. Morrison, C. J. Buckley, Eds. (Springer-Verlag, New York, 1992), pp. 75–78.
- H. N. Chapman, K. A. Nugent, S. W. Wilkins, T. J. Davis, *J. X-ray Sci. Technol.* **2**, 117 (1990).
- M. A. Kumakhov and F. F. Komarov, *Phys. Rep.* **191**, 289 (1990).
- D. A. Carpenter *et al.*, in *Microbeam Analysis—1988*, D. E. Newbury, Ed. (San Francisco Press, San Francisco, CA, 1988), p. 391.
- "Center For X-ray Optics—1989," *LBL-28001 UC-411* (University of California, Berkeley, CA, 1990), p. 4-15.
- W. B. Yun *et al.*, *Proc. Soc. Photo-Opt. Instrum. Eng.* **1740**, 117 (1993).
- A 0.8- μm beam at 15 keV has been made at the European Synchrotron Radiation Facility, Grenoble, France, from a Bragg Fresnel lens designed by A. Snigiriv and V. Aristov (C. Riekel, private communication).
- E. A. Stern, Z. Kalman, A. Lewis, K. Lieberman, *Appl. Opt.* **27**, 5135 (1988).
- P. Engstrom *et al.*, *Nucl. Instrum. Methods. Phys. Res. Sect. A* **302**, 547 (1991).
- D. J. Thiel, D. H. Bilderback, A. Lewis, E. A. Stern, *ibid.* **317**, 597 (1992).
- S. A. Hoffman, D. J. Thiel, D. H. Bilderback, *Opt. Eng.*, in press.
- D. H. Bilderback, *Proc. Soc. Photo-Opt. Instrum. Eng.* **315**, 90 (1981).
- D. Cooke *et al.*, *Nature* **346**, 802 (1990).
- K. T. Brown and D. G. Flaming, in *Advanced Micropipette Techniques for Cell Physiology*, A. D. Smith, Ed. (Wiley, New York, 1986), chap. 6.
- S. J. Andrews *et al.*, *Acta Crystallogr. Sect. A* **43**, 70 (1987).
- E. F. Skelton *et al.*, *Science* **253**, 1123 (1991).
- K. Ohsumi, K. Hagiya, M. Ohmasa, *J. Appl. Crystallogr.* **24**, 340 (1991).
- For providing the gold lithography sample, we thank R. Bojko and H. Craighead of the National Nanofabrication Facility, which is supported by NSF grant ECS-8619049, Cornell University, and industrial affiliates. We also acknowledge S. Ealick's group for the lysozyme sample and M. Fitzsimmons for the gold foil sample. This material is based upon work conducted at CHESS and supported by NSF grant DMR 90-21700 and NIH grant RR01646-10.

11 August 1993; accepted 9 November 1993

Free-Radical Side-Chain Bromination of Alkylaromatics in Supercritical Carbon Dioxide

James M. Tanko* and Joseph F. Blackert

Free-radical side-chain brominations of alkylaromatics in supercritical carbon dioxide (SC-CO₂) are reported. Direct bromination of toluene and ethylbenzene form the corresponding benzyl bromides in high yield. The observed selectivity in SC-CO₂ is similar to that observed in conventional organic solvents. Also, SC-CO₂ is an effective alternative to carbon tetrachloride for use in the classical Ziegler bromination with *N*-bromosuccinimide. Reaction yields are high, side products are minimized, and bromine-atom selectivities are observed. Thus, SC-CO₂ must be useful as a viable, environmentally benign substitute for many of the solvents typically used for free-radical reactions.

The need to reduce or eliminate toxic chemical wastes and by-products in chemical manufacturing requires the development of new synthetic methods that use compounds that are less toxic and more environmentally benign (1). For certain reactions, the solvents that have been selected for their chemical inertness are highly halogenated compounds that are not environmentally benign [such as chloroflu-

orocarbons (CFCs) and carbon tetrachloride (CCl₄)].

One such class of reactions are free-radical brominations of alkylaromatic compounds such as toluene. Reaction of molecular bromine with an alkylaromatic in a suitable solvent, initiated either photochemically or thermally with a free-radical initiator, produces the corresponding benzylic bromide in nearly quantitative yield. The mechanism of the reaction (Fig. 1) involves a free-radical chain process in which (i) hydrogen abstraction by atomic bromine (Br[•]) generates a benzylic radical (PhCH₂•)

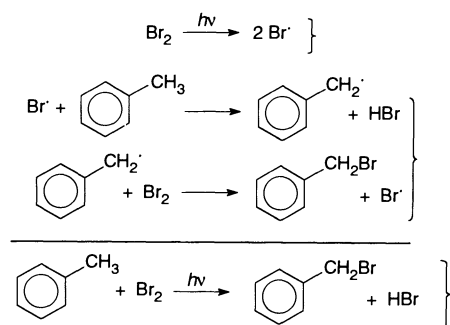


Fig. 1. Free-radical bromination of toluene. Initiated photochemically (top bracket; h is Planck's constant, ν is the frequency of the radiation), bromination propagates by the next two reactions (middle bracket). The overall reaction (bottom bracket) is shown below the summation line.

and HBr and (ii) trapping of PhCH₂• by molecular bromine produces benzyl bromide and regenerates Br[•]. Long chain lengths are observed for these reactions, and the selectivity associated with hydrogen abstractions by Br[•] is very high (generally the weakest C–H bond in the substrate is broken) (2).

Suitable solvents for this reaction (such as CFCs and CCl₄) must not have abstractable hydrogen atoms or reactive double bonds. An appropriate replacement solvent would be SC-CO₂ because of its virtual nontoxicity and its solvating properties (3). There are important issues that must be addressed in the assessment of the utility of SC-CO₂ as a solvent for radical reactions: Is SC-CO₂ inert toward free radicals? Are reaction yields compromised by the use of SC-CO₂? How are reactivity and selectivity affected in SC-CO₂ medium?

There have been few reports that address these issues. Leffler and co-workers reported that the decomposition of diacyl peroxides in SC-CO₂ yields products derived from both radicals and ion pairs (4). McHugh and co-workers reported the first example of a free-radical chain reaction in SC-CO₂, the oxidation of cumene (5). Fox, Johnston, and co-workers studied the dimerization of the benzyl radical (generated by photolysis of dibenzyl ketone in SC-CO₂) and noted a distinct absence of cage effects (6). Chateaufeuf and co-workers reported absolute rate constants for hydrogen-atom abstraction by triplet benzophenone from several donors and noted an intriguing effect of pressure (7). DeSimone and co-workers examined the kinetics of decomposition of the free-radical initiator 2,2'-azobis(isobutyronitrile) (AIBN) in SC-CO₂ and also reported the free-radical polymerization of 1,1-dihydroperfluorooctyl acrylate (FOA) (8).

We studied the reaction of Br₂ with toluene and ethylbenzene in SC-CO₂ (9) (Table 1). The major products of these reactions are the corresponding benzylic

Department of Chemistry, Virginia Polytechnic Institute and State University, Blacksburg, VA 24061-0212

*To whom correspondence should be addressed